REPRODUCED AT GOVERNMENT EXPENSE

(1)

SC5162.6AR

Copy No. 17

SC5162.6AR

TEMPERATURE COMPENSATED PIEZOELECTRIC MATERIALS

ANNUAL TECHNICAL REPORT
June 1, 1978 through May 31, 1979

AD-A149 218

GENERAL ORDER NO. 5162
CONTRACT NO. F49620-78-C-0093

DOCUMENT NO. SC5162.6AR

Prepared for

Air Force Office of Scientific Research
Bolling Air Force Base
Washington, D.C. 20332

DTIC
ELECTE
JAN 7 1985
S D
B

R. R. Neurgaonkar
Principal Investigator

AUGUST 1979

DTIC FILE COPY

Approved for public release: distribution unlimited

Rockwell International
Science Center

84 12 27 116

UNCLASSIFIED

SECURITY CLASSIFICATION OF THIS PAGE (When Data Entered)

REPORT DOCUMENTATION PAGE	READ INSTRUCTIONS BEFORE COMPLETING FORM
1 REPORT NUMBER	2. GOVT ACCESSION NO. AD-A149218 / 3 RECIPIENT'S CATALOG NUMBER
4 TITLE (and Subtitle) Temperature Compensated Piezoelectric Materials	5. TYPE OF REPORT & PERIOD COVERED Annual Report 6/1/78 thru 5/31/79
	6. PERFORMING ORG. REPORT NUMBER SC5162.6AR
7 AUTHOR(s) R. R. Neurgaonkar	8. CONTRACT OR GRANT NUMBER(s) F49620-78-C-0093
9. PERFORMING ORGANIZATION NAME AND ADDRESS Electronics Research Center Rockwell International Thousand Oaks, CA 91360	10. PROGRAM ELEMENT, PROJECT, TASK AREA & WORK UNIT NUMBERS ARPA Order No. 3570
11. CONTROLLING OFFICE NAME AND ADDRESS Air Force Office of Scientific Research Bolling Air Force Base Washington, D. C. 20332	12. REPORT DATE August, 1979
	13. NUMBER OF PAGES 54
14. MONITORING AGENCY NAME & ADDRESS (if different from Controlling Office) Director, Advanced Research Projects Agency 1400 Wilson Boulevard Arlington, VA 22209	15. SECURITY CLASS. (of this report) Unclassified
	15a. DECLASSIFICATION DOWNGRADING SCHEDULE

16. DISTRIBUTION STATEMENT (of this Report)

Approved for public release: distribution unlimited.

17. DISTRIBUTION STATEMENT (of the abstract entered in Block 20, if different from Report)

18. SUPPLEMENTARY NOTES

19 KEY WORDS (Continue on reverse side if necessary and identify by block number)

Strontium barium niobates	Gibb's energy functions
Liquid phase epitaxy	Phenomenological model
Czochraski Growth Technique	Piezoelectric constants

20 ABSTRACT (Continue on reverse side if necessary and identify by block number)

A literature survey of the known tungsten bronze structural family has been completed and compiled. A phenomenological model based on the Gibb's energy functions to explain the nature of temperature compensation in the bronze family has currently been developed. This work has been extended to specific bronze phases such as the tetragonal SBN and the orthorhombic PBN. Several flux systems have successfully been established for the liquid phase epitaxy (LPE) work of the SBN compositions. The LPE work has recently been initiated on SBN phases using substrates and barium vanadate as flux.

DD FORM 1 JAN 73 1473

UNCLASSIFIED

SECURITY CLASSIFICATION OF THIS PAGE When Data Entered

The SBN single crystals grown in our laborabory showed exceptionally strong piezoelectric activity in all poled samples of SBN crystals.

TEMPERATURE-COMPENSATED PIEZOELECTRIC MATERIALS

ANNUAL TECHNICAL REPORT
June 1, 1978 through May 31, 1979

ARPA Order No.	3570
Program Code:	8D10
Name of Contractor:	Rockwell International
Effective Date of Contract:	May 15, 1978
Contract Expiration Date:	May 14, 1980
Amount of Contract Dollars:	$372,101
Contract Number:	F49620-78-C-0093
Principal Investigators:	Dr. R. R. Neurgaonkar (805) 498-4545 Ext. 109 Professor L. E. Cross Pennsylvania State University (814) 865-1181
Program Manager:	Dr. E. J. Staples (805) 498-4545 Ext. 202

Sponsored by

Advanced Research Projects Agency (DOD)
ARPA Order No. 3570
Monitored by AFOSR under Contract No. F49620-78-C-0093

The views and conclusions contained in this document are those of the authors and should not be interpreted as necessarily representing the official policies, either expressed or implied, of the Defense Advanced Research Projects Agency or the U. S. Government.

public

Approved for release: distribution unlimited

Rockwell International

TABLE OF CONTENTS

TABLE OF CONTENTS (Cont'd)

Accession For
NTIS GRA&I ☑
DTIC TAB ☐
Unannounced ☐
Justification
By
Distribution/
Availability Codes
Dist | Avail and/or Special
A-1

DTIC COPY INSPECTED

LIST OF FIGURES

LIST OF TABLES

1.0 PROGRESS AND TECHNICAL REPORT SUMMARY

The objective of the present research investigations are to determine why known ferroelectric and ferroelastic materials are temperature compensated and predict such occurrences. Knowledge from such a determination will be used to grow and characterize suitable phases from the tungsten bronze family. The end goal is to develop high coupling, temperature compensated materials for minimum shift keyed surface wave filters.

Considerable progress has been made in several areas and it is discussed in detail in subsections of this report. A literature survey of the known tungsten bronze structural family has been completed and compiled. This information is to provide the data necessary for the development of a phenomenological model based on the Gibbs energy functions to explain the nature of temperature compensation in these types of phases. Over the past several months, the efforts (at Penn State University) have been concentrated on the simple ferroeletrics in the tungsten bronze family, i.e., materials in which the elastic Gibbs free energy ϕ and the order parameters η and ρ are always zero, and thus, all components of the terms ϕ_1 and ϕ_3 in Gibbs function $\Delta G = d_1(\eta\rho) + \phi_2(XP) + \phi_3(XP\eta\rho)$ are zero. The information obtained from these studies will provide adequate descriptions of dielectric, piezoelectric, elastic and thermal behavior of the simple ferroelectric phases. This work has been extended to specific bronze phases such as tetragonal $Sr_{1-x}Ba_xNb_2O_6$ and the orthorhombic $PbNb_2O_6$. The theoretical aspects of this work has been described in detail in Sections 3.1 to 3.3.

Solvent selection and experimental setup for the liquid phase epitaxy (LPE) work of $Sr_{1-x}Ba_xNb_2O_6$ (SBN) compositions have successfully been established. Several systems including BaV_2O_6-$Sr_{1-x}Ba_xNb_2O_6$, BaB_8O_{13}-$Sr_{1-x}Ba_xNb_2O_6$ and SrV_2O_6-$Sr_{1-x}Ba_xNb_2O_6$ have been found to be most suitable to develop epilayers of SBN compositions. This is an important step for this growth work and the LPE work is in progress. The Z-cut SBN substrates and the BaV_2O_6-$Sr_{1-x}Ba_xNb_2O_6$ system will be used for this process.

The SBN substrates used in the LPE thin film work have been produced

in our laboratory to provide continuous supply of substrate materials. This work has been supported under IR&D funds and the crystals of the composition $Sr_{.61}Ba_{.39}Nb_2O_6$ have been grown by the Czochralski method. The growth process has successfully been developed and, to date, it is possible to produce 1/2 inch in diameter and 4 inch long crystals. This is a significant accomplishment in the present work and thus a breakthrough for our program, for substrates are no longer a problem. The results of this research will be published in the Journal of Crystal Growth. The structural and ferroelectric properties of the $Sr_{.61}Ba_{.39}Nb_2O_6$ crystals have been studied and it was found to have an exceptionally strong piezoelectric activity in all poled samples of SBN crystals.

2.0 TUNGSTEN BRONZE FERROELECTRICS

2.1 Literature Survey

2.1.1 Introduction

The initial digest of the literature on the ferroelectric bronze family materials has amply confirmed the expected variety in the chemistry of the bronzes. With the considerable flexibility of the tetragonal bronze prototype, it is difficult to separate compounds from solid solutions, and a limited range of mixed oxide off stoichiometry is to be expected in all the compounds listed. For the purpose of these studies, we have chosen to list as separate compounds all chemically distinct compositions $A_xB_yC_z...O_{30}$, where x,y,z... are whole numbers.

So far, using the data compilation by Landolt Bornstein (Vol. 3 and 9), the Digest of the Literature on Dielectrics, and the ORNL literature guides as starting points, 80 separate ferroelectric bronze compounds have been identified and original literature has been traced for 68 of these compounds listed in Table I.

2.1.2 Organization of the Data

The purpose of the present data compilation is two-fold: i) to provide accessible structural information so that the range of choices for host and epitaxial film compositions can be rapidly evaluated, ii) for the phenomenological analysis and its extension to solid solution systems, the data base in properties which have been measured on well characterized single crystals of the end member compositions is fundamentally important.

With the escalating size and complexity of the listing of the bronze structure compounds, it was decided that translating and storing the data in computer format would be worthwhile. For the small extra effort required to put the data into this form, it is now possible to retabulate at will, sorting according to any particular physical parameter. In the tabulation given in Table I, for example, the compounds have been ordered in descending ferroelectric transition temperatures (T_c).

A second advantage of using the computer for this function is the availability of a number of excellent graphics packages for the PSU system. Further, since we shall be running much of the computation for the phenomenological analysis on the ADAGE systems which is hard-wire interfaced with the system 370 in our computation center, with appropriate storage techniques handling and processing of the property data should be greatly facilitated.

In the present phase, most of the available compound bronzes have been identified. The property information is now being taken from the original papers and cross-checked with subsequent studies wherever possible. Indication of this build-up is given in Table I (a-d).

2.1.3 Bronze Solid Solutions

The problem of handling the data for the many possible solid solutions in the bronze systems is our major concern in the first year of this contract. Unfortunately, much of the original data is for ceramic (polycrystal) systems so that property data are, as we expected, rather scarce. The major trends in dimensions, phase stability and Curie temperature are, however, available as starting points for the phenomenological analysis.

Table Ia

Tungsten-Bronze Compounds

COMPOUNDS	AVAILABLE DATA[2]										
	STR[1]	T_c (°C)	LATTICE CONSTANTS			THERM α_{ij}	ε_{ij}	P_s	PYRO p_i	PIEZO d_{ijk}	ELASTIC c_{ij}, s_{ij}
			a_o	b_o	c_o						
$PbNb_2O_6$	O	560	17.51	17.81	7.73	*	T				
$Ba_2NaNb_5O_{15}$	O	560	17.591	17.625	7.992	*	T			T	T
$Pb_2NaNb_5O_{15}$	O	531	17.606	17.928	3.856						
$Pb_2KNb_5O_{15}$	O	460	17.78	18.05	3.917		T			*	*
$K_3Li_2Nb_5O_{15}$	T	420	12.560		4.039		T				
$Ba_5NaNb_3TiO_{30}$	T	414	12.50		4.00		T	T			
$Ba_4Bi_2Fe_2Nb_8O_{30}$	T	400	12.53		3.960						
$Ba_2KNb_5O_{15}$	T	373	12.55		4.019			*			
$Ba_2Na_3YNb_{10}O_{30}$	T	306	12.41		3.924						
$Ba_5KNb_9RiO_{30}$	T	290	12.52		4.01		T				
$K_2TbNb_5O_{15}$	T	280	12.440		3.910						
$K_2DyNb_5O_{15}$	T	290	12.431		3.903						
$BaSrKNb_5O_{15}$	T	278	12.520		3.975						

1. T-Tetragonal, O-Orthorhombic
2. *-Data reported
   T-Data reported as a function of temperature
   x-Data reported as a function of composition

Table Ib

Tungsten-Bronze Compounds

COMPOUNDS	AVAILABLE DATA[2]										
	STR[1]	T_c (°C)	LATTICE CONSTANTS			THERM α_{ij}	ε_{ij}	P_s	PYRO p_i	PIEZO d_{ijk}	ELASTIC c_{ij}, s_{ij}
			a_o	b_o	c_o						
$BaSrNaNb_5O_{15}$	T	274	12.443		3.945			x			
$Sr_2NaNb_5O_{15}$	T	266					T				
$BaCaKNb_5O_{15}$	T	266	12.442		3.954						
$PbTa_2O_6$	O	265	17.68	17.72	7.754	*	T				
$K_2GdNb_5O_{15}$	T	250	12.450		3.912						
$Ba_2Na_2YNb_{10}O_{30}$	T	220	12.400		3.900						
$Ba_2Na_3DyNb_{10}O_{30}$	T	220	12.405		3.893						
$K_2EuNb_5O_{15}$	T	205	12.457		3.914						
$Ba_4Sr_2Nb_8Ti_2O_{30}$	T	200	12.44		3.94		*				
$K_2SmNb_5O_{15}$	T	195	12.474		3.917						
$Sr_4Ca_2Nb_8Ti_2O_{30}$	T	170	12.27		3.86		*				
$Ba_2Na_3CdNb_{10}O_{30}$	T	170	12.417		3.895						
$K_2NdNb_5O_{15}$	T	160	12.497		3.924						
$Ba_5NaNb_9TiO_{30}$	T	157	12.36		3.80		T				

1. T-Tetragonal, O-Orthorhombic
2. *-Data reported
   T-Data reported as a function of temperature
   x-Data reported as a function of composition

Table Ic

Tungsten-Bronze Compounds

COMPOUNDS	AVAILABLE DATA[2]										
	STR[1]	T_c (°C)	LATTICE CONSTANTS			THERM α_{ij}	ε_{ij}	P_s	PYRO p_i	PIEZO d_{ijk}	ELASTIC c_{ij}, s_{ij}
			a_o	b_o	c_o						
$Sr_2KNb_5O_{15}$	T	156	12.47		3.942		T	*			
$Ba_2Na_3EuNb_{10}O_{30}$	T	155	12.429		3.902						
$Ba_3NaYNb_{10}O_{30}$	T	145	12.423		3.933						
$Sr_2RbNb_5O_{15}$	T	139	12.51		3.949		*				
$Sr_6Nb_8Ti_2O_{30}$	T	130	12.36		3.89		T				
$Ba_3Gd_2Fe_2Nb_8O_{30}$	T	130									
$Ba_4Sm_2Fe_2Nb_8O_{30}$	T	130	12.46		3.926			*			
$BaSrNb_4O_{12}$	T	125	12.40		3.930	*	T,x	T	*	*	*
$Sr_5KNb_9TiO_{30}$	T	118	12.38		3.90		T				
$Sr_2KTa_5O_{15}$	O	110	17.550	17.660	3.890						
$Ba_4Ca_2Nb_8Ti_2O_{30}$	T	30	12.37		3.92		*				
$Ba_3NaGdNb_{10}O_{30}$	T	20	12.449		3.934						
$K_3Li_2Ta_5O_{15}$	O	7	17.78	17.83	3.931						
$Ba_2Na_3LaNb_{10}O_{30}$	T	-25	12.460		3.955						

1. T-Tetragonal, O-Orthorhombic
2. *-Data reported
   T-Data reported as a function of temperature
   x-Data reported as a function of composition

Table Id

Tungsten-Bronze Compounds

COMPOUNDS	AVAILABLE DATA[2]										
	STR[1]	T_c (°C)	LATTICE CONSTANTS			THERM α_{ij}	ε_{ij}	P_s	PYRO p_i	PIEZO d_{ijk}	ELASTIC c_{ij}, s_{ij}
			a_o	b_o	c_o						
$Ba_3NaLaNb_{10}O_{30}$	T	-50	12.475		3.950						
$K_2LaNb_5O_{15}$	T	-90	12.58		3.93						
$Rb_2LaNb_5O_{15}$	T	-120			3.945						
$BaNa_2Nb_5O_{14}F$	T		12.369		3.928						
$SrNb_2O_6$	T		17.720		7.760						
$BaNa_2La_2Nb_{10}O_{30}$	T		12.475		3.904						
$K_2CeNb_5O_{15}$	T		12.545		3.913						
$K_2PrNb_5O_{15}$	T		12.530		3.918						
$K_2HoNb_5O_{15}$	T		12.426		3.899						
$K_2YNb_5O_{15}$	T		12.424		3.901						
$Ba_2Nd_4Fe_3Nb_7O_{30}$	T		12.48		3.929		*				
$Ba_2Sm_4Fe_3Nb_7O_{30}$	T		12.46		3.93		*				
$Pb_2Nd_4Fe_3Nb_7O_{30}$	T		12.43		3.92		*				
$Bi_2Nd_4Fe_4Nb_6O_{30}$	T		12.54		3.86		*				

1. T-Tetragonal, O-Orthorhombic
2. *-Data reported
   T-Data reported as a function of temperature
   x-Data reported as a function of composition

3.0 THEORETICAL FORMULATION OF TEMPERATURE COMPENSATED FERROELECTRIC MATERIALS

3.1 Introduction

For the first year, the theoretical studies have been concentrated on simple ferroelectrics in the tungsten bronze family, i.e., materials in which the elastic Gibbs free energy, ϕ, the order parameters, η and ρ are always zero, and thus all components of the terms ϕ_1 and ϕ_3 in Gibbs function

$$\Delta G = \phi_1(\eta\rho) + \phi_2(XP) + \phi_3(XP\eta\rho) \tag{3.1}$$

are zero.

The objectives of these studies have been: a) to determine the level of expansion necessary to give an adequate description of the dielectric, piezoelectric, elastic, and thermal behavior of the simple ferroelectric phases, and b) to show bronzes which exhibit strong diffuse phase transitions (corresponding to a broad distribution of Curie temperatures), the static properties can be described by using a distribution of Curie temperatures in the phenomenological function.

3.2 Derivation of the Phenomenological Relationships

If the elastic Gibbs function may be written in the form

$$\begin{aligned}\Delta G = {} & \alpha_1(P_1^2 + P_2^2) + \alpha_3 P_3^2 + \alpha_{11}(P_1^4 + P_2^4) + \alpha_{33}P_3^4 \\ & + \alpha_{13}(P_1^2P_3^2 + P_2^2P_3^2) + \alpha_{12}P_1^2P_2^2 + \alpha_{333}P_3^6 \\ & + \alpha_{111}(P_1^6 + P_2^6) - \tfrac{1}{2}S_{11}(X_1^2 + X_2^2) - S_{12}X_1X_2 \\ & - S_{13}(X_1 + X_2)X_3 - \tfrac{1}{2}S_{33}X_3^2 - \tfrac{1}{2}S_{44}(X_4^2 + X_5^2) \\ & + Q_{13}(P_1^2X_3 + P_2^2X_3) + Q_{31}(P_3^2X_1 + P_3^2X_2)\end{aligned} \tag{3.2}$$

$$+ Q_{33}(P_3^2 X_3) + Q_{44}(P_2 P_3 X_4 + P_1 P_3 X_5)$$

$$+ Q_{66} P_1 P_2 X_6$$

The first partial derivatives with respect to the polarization give the field components

$$\frac{\partial \Delta G}{\partial P_1} = E_1 = 2\alpha_1 P_1 + 4\alpha_{11} P_1^3 + 2\alpha_{13} P_1 P_3^2$$

$$+ 2\alpha_{12} P_1 P_2^2 + 6\alpha_{111} P_1^5$$

$$+ Q_{13} P_1 X_3 + Q_{44} P_3 X_5 + Q_{66} P_1 X_6$$

$$\frac{\partial \Delta G}{\partial P_2} = E_2 = 2\alpha_1 P_2 + 4\alpha_{11} P_2^3 + 2\alpha_{13} P_2 P_3^2$$

$$+ 2\alpha_{12} P_2 P_1^2 + 6\alpha_{111} P_2^5 \qquad (3.3)$$

$$+ 2Q_{13} P_2 X_3 + Q_{44} P_3 X_4 + Q_{66} P_1 X_6$$

$$\frac{\partial \Delta G}{\partial P_3} = E_3 = 2\alpha_3 P_3 + 4\alpha_{33} P_3^3 + 2\alpha_{13}(P_1^2 + P_2^2) P_3$$

$$+ 6\alpha_{333} P_3^5 + 2Q_{31} P_3 (X_1 + X_2)$$

$$+ 2Q_{33} P_3 X_3 + Q_{44}(P_2 X_4 + P_1 X_5)$$

and the second derivatives therefore give the isothermal dielectric stiffness

$$\frac{\partial^2 \Delta G}{\partial P_1^2} = \frac{\partial E_1}{\partial P_1} = X_{11} = 2\alpha_1 + 12\alpha_{11} P_1^2 + 2\alpha_{13} P_3^2 + 2\alpha_{12} P_2^2$$

$$+ 30\alpha_{111} P_1^4 + 2Q_{13} X_3$$

$$\frac{\partial^2 \Delta G}{\partial P_2^2} = \frac{\partial E_2}{\partial P_2} = X_{22} = 2\alpha_1 + 12\alpha_{11}P_2^2 + 2\alpha_{13}P_3^2 + 2\alpha_{12}P_1^2$$

$$+ 30\alpha_{111}P_1^4 + 2Q_{13}X_3 \qquad (3.4)$$

$$\frac{\partial^2 \Delta G}{\partial P_3^2} = \frac{\partial E_3}{\partial P_3} = X_{33} = 2\alpha_3 + 12\alpha_{33}P_3^2 + 2\alpha_{13}(P_1^2+P_1^2)$$

$$+ 30\alpha_{333}P_3^4 + 2Q_{31}(X_1+ X_2)$$

$$+ 2Q_{33}X_3$$

$$\frac{\partial 2_{\Delta G}}{\partial P_1 \partial P_2} = \frac{\partial E_1}{\partial P_2} = X_{12} = 4\alpha_{12}P_1P_2$$

$$\frac{\partial 2_{\Delta G}}{\partial P_1 \partial P_3} = \frac{\partial E_1}{\partial P_3} = X_{13} = 4\alpha_{13}P_1P_3 + Q_{44}X_5$$

$$\frac{\partial 2_{\Delta G}}{\partial P_2 \partial P_3} = \frac{\partial E_2}{\partial P_3} = X_{23} = 4\alpha_{13}P_2P_3 + Q_{44}X_4$$

In many cases, for higher frequency AC behavior, the adiabitic stiffnesses are required. If, as will be the case for the simplified description, only α_1 and α_3 are functions of temperature T and take the form

$$\alpha_1 = \alpha_{10}\ (T-\theta_1) \text{ and } \alpha_3 = \alpha_{30}\ (T-\theta_3)$$

In this case, the adiabatic correction which is given simply by

$$\left(\frac{\partial E}{\partial P}\right)_S = \left(\frac{\partial E}{\partial P}\right)_T + \left(\frac{\partial E}{\partial T}\right)_P^2 \Big/ \left(\frac{\partial S}{\partial T}\right)_P \qquad (3.5)$$

takes the form

$$\left(\frac{\partial E_1}{\partial T}\right)_P = 2\alpha_{10}P_1$$

$$\left(\frac{\partial E_2}{\partial T}\right)_P = 2\alpha_{10}P_2 \qquad (3.6)$$

$$\left(\frac{\partial E_3}{\partial T}\right)_P = 2\alpha_{30}P_3$$

Orthorhombic solution $P_1^2 = P_2^2 \neq 0 \quad P_3^2 = 0$

$$E_1 = 2\alpha_1 P_1 + (4\alpha_{11} + 2\alpha_{12})P_1^3 + 6\alpha_{111}P_1^5 + 2Q_{13}P_1X_3 + Q_{66}P_1X_6$$

$$E_2 = 2\alpha_1 P_1 + (4\alpha_{11} + 2\alpha_{12})P_1^3 + 6\alpha_{111}P_1^5 + 2Q_{13}P_1X_3 + Q_{66}P_1X_6$$

$$E_3 = Q_{44}P_1(X_4 + X_5)$$

Spontaneous states

$$P_1 = 0 \text{ or } 0 = 2\alpha_1 + (4\alpha_{11} + 2\alpha_{12})P_1^2 + 6\alpha_{111}P_1^4$$

$$P_2 = 0 \text{ or } 0 = 2\alpha_1 + (4\alpha_{11} + 2\alpha_{12})P_1^2 + 6\alpha_{111}P_1^4$$

$$P_3 = 0$$

Dielectric stiffnesses (pseudomonoclinic axes)

$$x_{11} = 2\alpha_1 + 12\alpha_{11}P_1^2 + 2\alpha_{12}P_1^2 + 30\alpha_{111}P_1^4$$

$$x_{22} = 2\alpha_1 + 12\alpha_{11}P_1^2 + 2\alpha_{12}P_1^2 + 30\alpha_{111}P_1^4 \qquad (3.7)$$

$$x_{33} = 2\alpha_3 + 4\alpha_{13}P_1^2$$

$$x_{12} = 4\alpha_{12}P_1^2$$

Adiabatic stiffnesses

$$\chi_{11} = 2\alpha_1 + (12\alpha_{11} + 2\alpha_{12})P_1^2 + 30\alpha_{111}P_1^4 + 4\alpha_{10}{}^2P_1^2 \frac{T}{CP}$$

$$\chi_{22} = 2\alpha_1 + (12\alpha_{11} + 2\alpha_{12})P_1^2 + 30\alpha_{111}P_1^4 + 4\alpha_{10}{}^2P_1^2 \frac{T}{CP} \qquad (3.8)$$

$$\chi_{33} = 2\alpha_3 + 4\alpha_{13}P_1^2$$

$$\chi_{12} = 4\alpha_{12}P_1^2 + 4\alpha_{10}{}^2P_1^2 \frac{T}{CP}$$

The elastic strains are given by the negative of the partial derivatives of ΔG with respect to the components of stress as follows:

$$\frac{\partial G_1}{\partial X_1} = -x_1 = -S_{11}X_1 - S_{12}X_2 - S_{13}X_3 + Q_{11}P_1^2 + Q_{12}P_2^2 + Q_{31}P_3^2$$

$$\frac{\partial G_1}{\partial X_2} = -x_2 = -S_{11}X_2 - S_{12}X_1 - S_{13}X_3 + Q_{11}P_2^2 + Q_{12}P_1^2 + Q_{31}P_3^2$$

$$\frac{\partial G_1}{\partial X_3} = -x_3 = -S_{13}(X_1 + X_2) - S_{33}X_3 + Q_{13}(P_1^2 = P_2^2) + Q_{33}P_3^2$$

$$\frac{\partial G_1}{\partial X_4} = -x_4 = -S_{44}X_4 + Q_{44}P_2P_3 +$$

$$\frac{\partial G_1}{\partial X_5} = -x_5 = -S_{44}X_5 + Q_{44}P_1P_3$$

$$\frac{\partial G_1}{\partial X_6} = -x_6 = -S_{66}X_6 + Q_{66}P_1P_2 \qquad (3.9)$$

Orthorhombic spontaneious strains $P_1^2 = P_2^2 \neq 0$ $P_3 = 0$ $X_{1\to6} \equiv 0$

$$-x_1 = (Q_{11} + Q_{12})P_1^2$$

$$-x_2 = (Q_{11} + Q_{12})P_1^2$$

$$-x_3 = 2Q_{13}P_1^2$$

$$-x_4 = 0$$

$$-x_5 = 0$$

$$-x_6 = Q_{66}P_1^2$$

Similarly, the piezoelectric b coefficients are expressed by the second partial derivative of G with respect to X and P in the form

$$\frac{\partial x_1}{\partial P_1} = b_{11} = -2Q_{11}P_1 \qquad \frac{\partial x_1}{\partial P_2} = b_{21} = -2Q_{12}P_2 \qquad \frac{\partial x_1}{\partial P_3} = b_{31} = -2Q_{31}P_3$$

$$\frac{\partial x_2}{\partial P_1} = b_{12} = -2Q_{12}P_2 \qquad \frac{\partial x_2}{\partial P_2} = b_{22} = -2Q_{11}P_2 \qquad \frac{\partial x_2}{\partial P_3} = b_{32} = -2Q_{31}P_3$$

$$\frac{\partial x_3}{\partial P_1} = b_{13} = -2Q_{13}P_1 \qquad \frac{\partial x_3}{\partial P_2} = b_{23} = -2Q_{13}P_2 \qquad \frac{\partial x_3}{\partial P_3} = b_{33} = -2Q_{33}P_3 \qquad (3.10)$$

$$\frac{\partial x_4}{\partial P_1} = b_{14} = -2Q_{144}P_1P_2P_3 \qquad \frac{\partial x_4}{\partial P_2} = b_{24} = -Q_{44}P_3 \qquad \frac{\partial x_4}{\partial P_3} = b_{34} = -Q_{44}P_2$$

$$\frac{\partial x_5}{\partial P_1} = b_{15} = -Q_{44}P_3 \qquad \frac{\partial x_5}{\partial P_2} = b_{25} = -2Q_{144}P_1P_2P_3 \qquad \frac{\partial x_5}{\partial P_2} = b_{35} = -Q_{44}P_1$$

$$\frac{\partial x_6}{\partial P_1} = b_{16} = -Q_{66}P_2 \qquad \frac{\partial x_6}{\partial P_2} = b_{26} = -Q_{66}P_1 \qquad \frac{\partial x_6}{\partial P_3} = b_{36} = -2Q_{366}P_1P_2P_3$$

$$
\begin{aligned}
b_{11} &= -2Q_{11}P_1 & b_{21} &= -2Q_{12}P_1 & b_{31} &= 0 \\
b_{12} &= -2Q_{12}P_1 & b_{22} &= -2Q_{11}P_1 & b_{32} &= 0 \\
b_{13} &= -2Q_{13}P_1 & b_{23} &= -2Q_{13}P_1 & b_{33} &= 0 \\
b_{14} &= 0 & b_{24} &= 0 & b_{24} &= -Q_{44}P_1 \\
b_{15} &= 0 & b_{25} &= 0 & b_{35} &= -Q_{44}P_1 \\
b_{16} &= -Q_{66}P_1 & b_{26} &= -Q_{66}P_1 & b_{36} &= 0
\end{aligned}
\qquad (3.11)
$$

$$
\begin{matrix}
b_{11} & b_{12} & b_{13} & 0 & 0 & b_{16} \\
b_{21} & b_{22} & b_{23} & 0 & 0 & b_{26} \\
0 & 0 & 0 & b_{34} & b_{35} & 0
\end{matrix}
$$

In general, there are seven possible ferroelectric species which can occur from the prototypic 4/mmm symmetry of the paraelectric phase of the tungsten bronze, each of which corresponds to a different combination of non-zero (spontaneous) values of the P_i components. Practically, however, just two of these solutions encompass all presently known simple ferroelectric bronzes. These are

$$\text{(a) } P_3^2 \neq 0 \quad P_1 = p_2 = 0; \quad \text{(b) } P_1^2 = P_2^2 \neq 0 \quad P_3 = 0 \qquad (3.12)$$

The species (a) has domains in point symmetry 4mm and corresponds to Shuvalov[1] species 4mmm(1)D4F4mm.11 with two equivalent polar states $\pm P_S$ along the 4 fold prototypic axis. The second species (b) is one of the two subtypes of 4mmm(2)D2Fmm2.11, with P_S along the 2 fold axis, which make angles of 45° with the 1 and 2 prototype axes ($P_1^2 = P_2^2$) and four equivalent ferroelectric domain states.

Substituting the conditions (a) into the general equations derived

above gives the following conditions for stability:

$$P_1 = P_2 = 0 \qquad 0 = 2\alpha_3 + 4\alpha_{33}P_3^2 + 6\alpha_{333}P_3^5 \tag{3.13}$$

The isothermal dielectric stiffnesses are

$$\begin{aligned} x_{11}^T &= 2\alpha_1 + 2\alpha_{13}P_3^2 \\ x_{22}^T &= 2\alpha_1 + 2\alpha_{13}P_3^2 \\ x_{33}^T &= 2\alpha_3 + 2\alpha_{33}P_3^2 + 30\alpha_{333}P_3^4 \\ x_{12}^T &= x_{13} = x_{23} = 0 \end{aligned} \tag{3.14}$$

The adiabatic stiffnesses are

$$\begin{aligned} x_{11}^S &= 2\alpha_1 + 2\alpha_{13}P_3^2 \\ x_{22}^S &= 2\alpha_1 + 2\alpha_{13}P_3^2 \\ x_{33}^S &= 2\alpha_3 + 12\alpha_{33}P_3^2 + 30\alpha_{333}P_3^4 + 4\alpha_{30}P_3^2 \quad \text{T/CP} \end{aligned} \tag{3.15}$$

The tetragonal spontaneous strains are given by

$$\begin{aligned} -x_1 &= Q_{31}P_3^2 \qquad x_4 = x_5 + x_6 = 0 \\ -x_2 &= Q_{31}P_3^2 \\ -x_3 &= Q_{33}P_3^2 \end{aligned} \tag{3.16}$$

and the piezoelectric b coefficients by

$$b_{11} = 0 \qquad b_{21} = 0 \qquad b_{31} = -2Q_{31}P_3$$

$$b_{12} = 0 \qquad b_{22} = 0 \qquad b_{32} = -2Q_{31}P_3$$

$$b_{13} = 0 \qquad b_{23} = 0 \qquad b_{33} = -2Q_{33}P_3 \qquad (3.17)$$

$$b_{14} = 0 \qquad b_{24} = -Q_{44}P_3 \qquad b_{34} = 0$$

$$b_{15} = -Q_{44}P_3 \qquad b_{25} = 0 \qquad b_{35} = 0$$

$$b_{16} = 0 \qquad b_{26} = 0 \qquad b_{36} = 0$$

For the case (b), the corresponding equations take for form, for the stability conditions

$$P_1^2 = P_2^2 \qquad 0 = 2\alpha_1 + (4\alpha_{11} + 2\alpha_{12})P_1^2 + 6\alpha_{111}P_1^4$$

$$P_3 = 0 \qquad (3.18)$$

Isothermal stiffnesses are

$$x_{11}^T = 2\alpha_1 + 2\alpha_{11}P_1^2 + 2\alpha_{12}P_1^2 + 30\alpha_{111}P_1^4$$

$$x_{22}^T = 2\alpha_1 + 2\alpha_{11}P_1^2 + 2\alpha_{12}P_1^2 + 30\alpha_{111}P_1^4 \qquad (3.19)$$

$$x_{33}^T = 2\alpha_3 + 4\alpha_{13}P_1^2$$

$$x_{34}^T = 4\alpha_{12}P_1^2 \qquad x_{13} = x_{23} = 0$$

and for the adiabatic coefficients

$$x_{11}^S = x_{11}^T + 4\alpha_{10}^2 P_1^2 T/CP$$

$$x_{22}^{S} = x_{22}^{T} + 4\alpha_{10}\,{}^{2}P_1^{\,2}\,T/CP$$

$$x_{33}^{S} = x_{33}^{T} \qquad (3.20)$$

$$x_{12}^{S} = x_{12}^{T} + 4\alpha_{10}\,{}^{2}P_1^{\,2}\,T/CP$$

It may be noted that the coefficients here are expressed with respect to the original prototypic axes and thus satisfy pseudomonoclinic symmetry. However, a simple rotation of the matrix by 45° in the 1,2 plane would reveal the true orthorhombic symmetry.

Spontaneous elastic strains take for form

$$-x_1 = (Q_{11} + Q_{12})P_1^{\,2}$$

$$-x_2 = (Q_{11} + Q_{12})P_1^{\,2} \qquad (3.21)$$

$$-x_3 = 2Q_{13}P_1^{\,2}$$

$$-x_6 = Q_{66}P_1^{\,2} \qquad x_4 = x_5 = 0$$

and the piezoelectric coefficients are

$$b_{11} = -2Q_{11}P_1 \qquad b_{21} = -2Q_{12}P_1 \qquad b_{31} = 0$$

$$b_{12} = -2Q_{12}P_1 \qquad b_{22} = -2Q_{11}P_1 \qquad b_{32} = 0$$

$$b_{13} = -2Q_{13}P_1 \qquad b_{23} = -2Q_{13}P_1 \qquad b_{33} = 0 \qquad (3.22)$$

$$b_{14} = 0 \qquad b_{24} = 0 \qquad b_{34} = -Q_{44}P_1$$

$$b_{15} = 0 \qquad b_{25} = 0 \qquad b_{35} = -Q_{44}P_1$$

$$b_{16} = -Q_{66}P_1 \qquad b_{26} = Q_{66}P_1 \qquad b_{36} = 0$$

The relationships derived above contain the following implicit assumptions:

a) The Taylor series expansion of ΔG contains all allowed terms up to 4th power, but only the first sixth power terms in polarization.

b) The coefficients α_1 and α_3 carry the major temperature dependence and have the form

$$\alpha_1 = \alpha_{10}(T-\theta_1) \text{ and } \alpha_3 = \alpha_{30}(T-\theta_3)$$

c) The coefficients α_{10}, α_{30}, and all higher order coefficients are constants for any given bronze composition and do not change in magnitude at the paraelectric:ferroelectric transition.

3.3 Applications of the Phenomenology

3.3.1 General Observations

The essential requirements which make it possible to use the phenomenological relationships in a predictive manner are: a) that the temperature independent constants maintain rather similar values across many different compositions with the same prototype structure, b) within a given solid solution family, both the lowest order and the highest order stiffness terms mutate only slowly and continuously with changing composition.

Experience within a very wide range of perovskite structure ferroelectrics has shown that the above conditions are satisfied in this family of oxygen octahedron ferroelectrics. In the tungsten bronze structure materials, we note:

a) for the prototype symmetry, seven different ferroic species are possible, yet within all bronzes that have studied to date, only two species are, in fact, found. This must imply that there are a number of special relationships between magnitudes in the higher order terms dictated by the

bonding in the bronzes, which are preserved across the whole vast family of bronze compositions. For example, it may be expected that since solution $P_1^2 = P_2^2 \neq 0$, $P_3^3 = 0$ occurs, but $P_1^2 \neq 0$, $p_2^2 = P_3^2 = 0$ does not, the coefficient α_{12} must always be negative. Similarly, since solutions involving non-zero values of P_1 and P_3 do not occur in the bronzes, though they can in the bismuth oxide layer structure family which have the same prototype symmetry, it is expected that α_{13} is positive.

Since the solutions (a) and (b) are not symmetry related, it may be expected that they are controlled by different mode softening and we postulte $\alpha_1 = \alpha_{10}(T-\theta_1)$ $\alpha_3 = \alpha_{30}(T-\theta_3)$.

Clearly, if $\theta_1 > \theta_3$ and α_{12} is negative, the orthorhombic solution (b) will occur for temperatures less than θ_1, while if $\theta_3 > \theta_1$, the tetragonal solution (a) will pre-empt the ferroelectricity.

The task is then to determine the constants for as wide a range of the tetragonal and orthorhombic bronze structures as possible, to determine the range of each parameters and the adequacy of the phenomenological expansion. Unfortunately, we find the difficulty of this task compounded by the exceedingly "spotty" experimental information. For no ferroelectric bronze are there really adequate and complete measurements which would permit simple verification and cross-checking. Thus, it is necessary in many cases to resort to indirect approaches. Two examples of the type of study being accomplished are:

3.3.2 Determination of the Phenomenological Constants for $PbNb_2O_6$

Lead metaniobate was one of the first tungsten bronze structure ferroelectrics to be studied, and there are extensive dielectric, some piezoelectric, and a little elastic data available which have been measured on single crystal samples.[1] In the solid solution system with $BaNb_2O_6$, there is a morphotropic boundary occurring at a composition near 0.35 mole% $BaNb_2O_6$ separating an orthorhombic (b) type species in the lead-rich compounds from a tetragonal (a) type species in the barium-rich compositions.

The T_c for orthorhombic ferroelectric phase decreases linearly with

Ba content up to 0.35 mole%, while after that composition, the Curie temperature T_c for the tetragonal phase (a) increases continuously. Extrapolating this tetragonal phase back to pure $PbNb_2O_6$ suggesta a θ_3 ≈276 in this material.

In the paraelectric phase of pure $PbNb_2O_6$, the dielectric stiffness should be given by

$$\chi_{11} = 2\alpha_{10}(T-\theta_1)$$

and

$$\chi_{33} = 2\alpha_{30}(T-\theta_3)$$

Curve fitting to these data gives

$$\alpha_{10} = 3.58\times10^6 \quad \alpha_{30} = 3.9\times10^6$$

$$\theta_1 = 550 \qquad \theta_3 = 280$$

Thus, there is good agreement between the two θ_3 values derived.

Now we may make use of the relations (3.19) and (3.20) to derive from th measured ε_a, ε_b, and ε_c values of the single domain single crystal values for the higher order stiffnesses.

This process is illustrated for α_{13}, which may be derived from the relation

$$\chi_{33}^{S} = \chi_{33}^{T} = 2\alpha_{30}(T-\theta_3) + 4\alpha_{13}P_1^2$$

giving values of $\alpha_{13} = 25\alpha_{30}$.

Similar direct and indirect applications of the phenomenological relations are being applied in a range of bronze compositions to build up values and value ranges for the higher order terms in the phenomenological expansion.

3.3.3 Diffuse Phase Transitions

A problem with many of the tungsten bronze composition which may be of interest for these studies is that they exhibit diffuse or broadened ferroelectric phase transitions. This phenomenon is attributed to short-range compositional heterogeneity giving rise to a distribution of local Curie temperatures.

The phenomenon is most obviously exhibited in a rounding off of the sharp changes in ϵ and P, which are associated with the first-order ferroelectric phase change.

As a first approach to a thermodynamic treatment for the mere diffuse materials, we have been experimenting with using a Gaussian distribution function to describe the smearing of Curie temperatures, and with calculating the response function as the sum of responses for the individual volume fractions in each state.

The simple example given here (Fig. 1) shows the curve-fit results for $Ba_{.5}Sr_{.5}Nb_2O_6$. The best fit was obtained for a Gaussian distribution function which has a half-width of 8°C.

Rather than remeasure the many P_S vs T curves in the literature, a technique has been developed to digitize the plots directly from the publications. These data are then used with a genrealized curve-fit program to determine the approximate temperature distribution of the phase transition. The x-axis and y-axis scales in Fig. 1 are dimensionaless, and were chosen because they could be readily applied to a variety of materials.

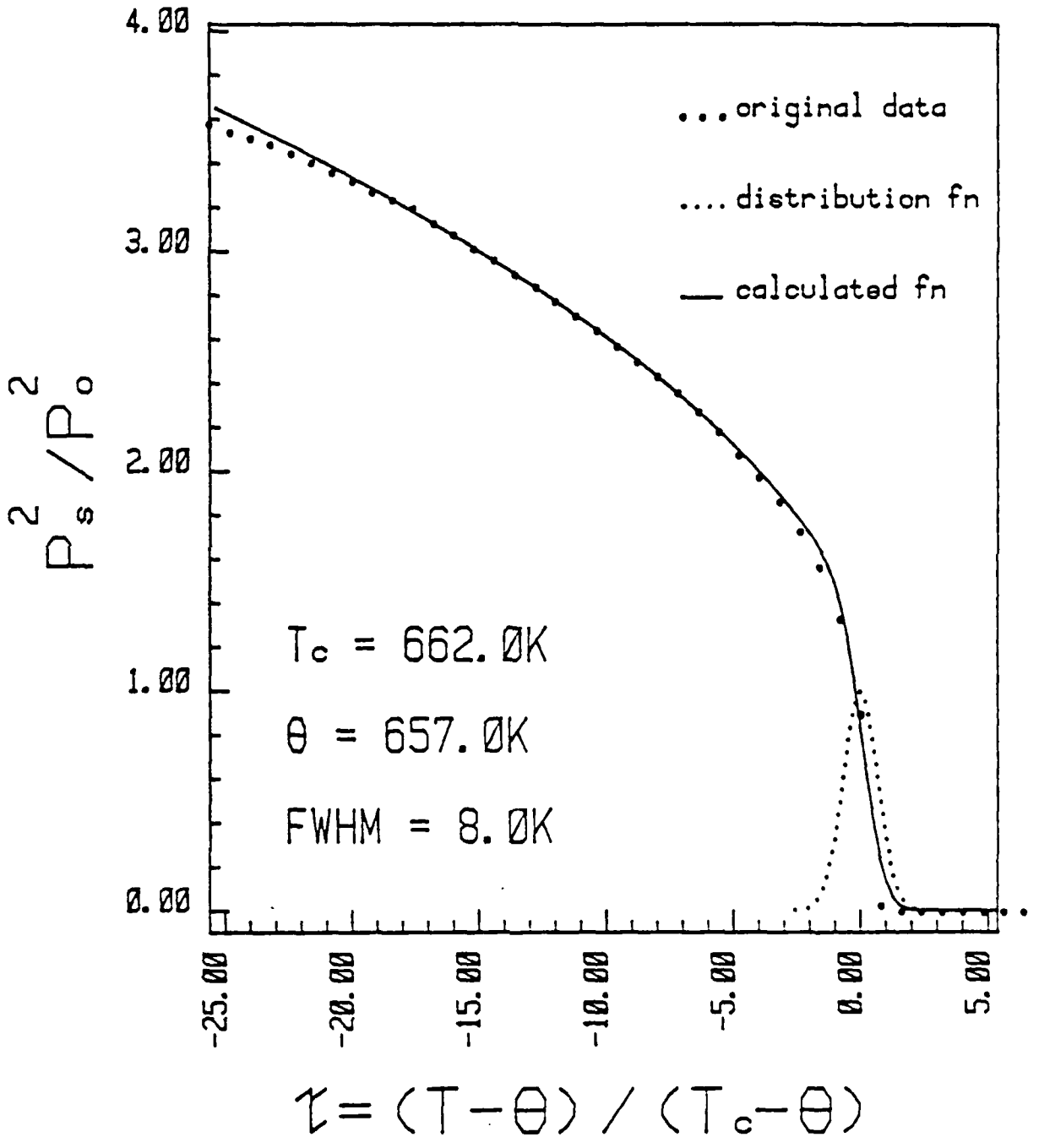

Fig. 1 Calculated plot of spontaneous polarization as a function of temperature.

4.0 MATERIAL GROWTH RESULTS

4.1 Apparatus and Flux Systems

A specific task of this contract is to establish techniques and construct suitable apparatus for liquid phase epitaxial (LPE) growth of selected materials identified in the above literature survey. A LPE furnace, described in Section 4.1.1 and its associated controls were constructed. As a result of the above literature survey, it was decided that the first member of the tungsten-bronze family to be studied would be strontinum-barium-niobate (SBN or $Sr_{1-x}Ba_xNb_2O_6$). Studies were then made to find suitable flux systems for the LPE growth of SBN. These fluxes are described in Section 4.1.2. The compositional range, x, for SBN is exceptionally large, $0.25 \leq$ to ≤ 0.75. The crystal chemistry of new tungsten-bronze solid-solutions that might be expected from element substitutions is discussed in Section 4.2

4.1.1 LPE Growth Apparatus

During the first part of this investigation, the LPE growth apparatus shown in Fig. 2 was constructed. The basic furnace consisted of a vertical platinum-wound resistance furnace capable of reaching 1500°C. It has an overall length of 20 inches with 2-1/2 inches internal diameter and external shunts at 2-inch intervals for adjusting the temperature profile. The temperature control system consists of an SCR power supply, high-stability supply controller (±0.2°C), and a temperature ramp generator for linearly varying the growth temperature up or down from 0.1 to 10°C/minute. Growth temperature is carefully monitored by placing two 90%-10% Rh-Pt thermocouples, one inside the other outside the melt. The system also contains a substrate preheating furnace, 600-700°C, located above the growth chamber, which isolates the substrate from any undesirable vapor during a preheating period. A lead-screw drive is used to lower or raise the substrate assembly holder through a predetermined distance from the top of the furnace to the appropriate immersion depth in the melt. This system is capable of traveling as slow as one inch per 20 minutes up or down, and rotating at 0.1 to 10 rps.

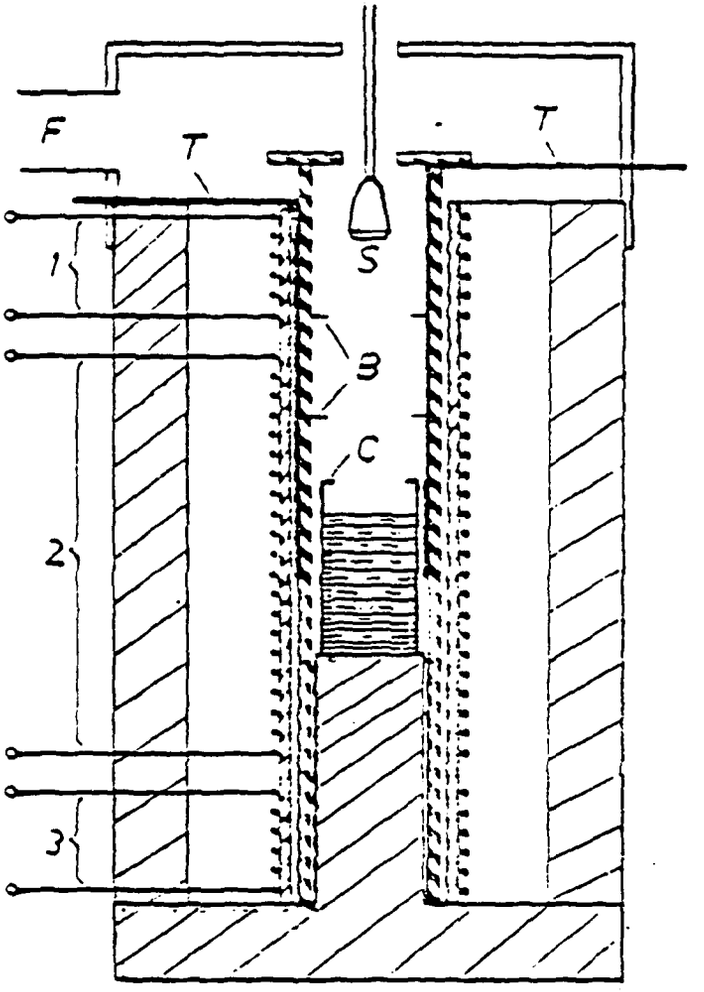

Fig. 2 Diagram of furnace for liquid phase epitaxy.

4.1.2 Tungsten-Bronze Solvents

In order to grow films by LPE, a suitable solvent flux must be found. The following information is being studied:

1. Liquidus temperature as a function of composition.
2. Crystallization range of the phase to be crystallized and its stability at elevated temperature.
3. Viscosity as a function of composition and growth temperature.
4. Density as a function of composition and growth temperature.

In order to grow high-quality films, these parameters must be known. Since the present systems contain five or more components, the determination of a complete phase diagram in such a situation is impractical. As described by Roy and White,[2] such systems can be treated as a pseudo-binary system with the phase to be crystallized as one component (solute) and the flux (solvent) as the other. Using this concept, several flux systems have been investigated for tungsten-bronze crystals. In particular, our goal was to crystallize the tungsten-bronze phase having the composition $Sr_{1-x}Ba_xNb_2O_6$. Table II documents the melting temperature, eutectic temperature and crystallization range for the flux systems thus far studied.

Our initial results indicated that the oxides of V_2O_5 and MO_3, where M = Mo or W, were very volatile when incorporated as flux. Their use has been discontinued and the alkali or alkaline earth vanadates and tungstates are now being used to determine the crystallization range of $Sr_{1-x}Ba_xNb_2O_6$. The $LiVO_3$, K_2WO_4, Li_2WO_4 and KVO_3 fluxes are relatively known and have been used by ourselves as well as others to grow $LiNbO_3$ films.[3-5]

Table II

Solvents for the Tungsten-Bronze Compounds

System	Melting Temp (°C) of Flux	Eutectic Temp. (°C)	Phases Present	Remarks
BaV_2O_6-$Sr_{1-x}Ba_xNb_2O_6$	700	685	SBN + BaV_2O_6	Long-useful crystallization range
BaB_8O_{13}-$Sr_{1-x}Ba_xNb_2O_6$	890	---	SBN + BaV_2O_6	Long-useful crystallization range
SrV_2O_6-$Sr_{1-x}Ba_xNb_2O_6$	750	---	SBN + SrV_2O_6	Long-useful crystallization range
KVO_3-$Sr_{1-x}Ba_xNb_2O_6$	520	490	SKN + Unknown	Long-useful crystallization range
$NaVO_3$-$Sr_{1-x}Ba_xNb_2O_6$	630	~560	SNN + Unknown	Long-useful crystallization range
V_2O_5-$Sr_{1-x}Ba_xNb_2O_6$	690	---	SBN + Unknown	Short-not suitable
K_2WO_4-$Sr_{1-x}Ba_xNb_2O_6$	920	---	TB + Unknown	Composition is not known
$LiVO_3$-$Sr_{1-x}Ba_xNb_2O_6$	700	---	$LiNbO_3$ + Unknown	Not suitable

1) SBN → $Sr_{1-x}Ba_xNb_2O_6$ has tetragonal tungsten bronze structure.
2) SKN → $Sr_2KNb_5O_{15}$ has tetragonal tungsten bronze structure.
3) SNN → $Sr_2NaNb_5O_{15}$ has tetragonal tungsten bronze structure.

For the determination of crystallization range of the $Sr_{1-x}Ba_xNb_2O_6$ tungsten bronze phase in the different systems, several specimens of different compoistions were prepared by mixing oxides, carbonates or nitrates in the required proportions. sufficiently mixed powders were slowly heated beyond the melting temperature in a platinum dish for a few minutes, and then quenched rapidly to room temperature. The specimen thus prepared was crushed into fine powder and then the flux was washed away with either water or dil. acids (HCl or HNO_3). The residual products was carefully studied by the x-ray powder diffraction technique. The results of this study indicated that the tetragonal tungsten bronze phase $Sr_{1-x}Ba_xNb_2O_6$ can easily be crystallized as a stable phase from the BaV_2O_6-$Sr_{1-x}Ba_xNb_2O_6$, SrV_2O_6-$Sr_{1-x}Ba_xNb_2O_6$, and BaB_8O_{13}-$Sr_{1-x}Ba_xNb_2O_6$ systems. Further, it has been found that the $Sr_{1-x}Ba_xNb_2O_6$ phase exists over a very wide compositional range in all three systems.

Since the tetragonal tungsten bronze structure extends over a wide compositional range ($0.25<x<0.75$) on the $SrNb_2O_6$-$BaNb_2O_6$ system,[6] it is very important to establish the Sr:Ba ratio for each composition crystalized from the BaV_2O_6-$Sr_{1-x}Ba_xNb_2O_6$ system. This has been accomplished by establishing the lattice constants a_A and cA for each composition, and then these constants were compared with known reported for the $Sr_{1-x}Ba_xNb_2O_6$ solid solution system. Figure 3 shows the variations in the lattice constants a_A and c_A for the $Sr_{1-x}Ba_xNb_2O_6$ solid solutions prepared in this work by the solid state reactions technique. It was found that the lattice constant c_A is much more sensitive as compared to the lattice constant a_A to determine the Sr:Ba ratio in the final phase. Table III summarizes the results of this work.

The work on the BaV_2-$_6$-$Sr_{1-x}Ba_xNb_2O_6$ system was continued to establish the composition-temperature relation using the differential thermal analysis (DTA) technique. Since the present system contains five or more components, the determination of a complete phase diagram in such a situation is impractical. Therefore, the system was treated as pseudo-binary. Figure 4 shows a composition-temperature relation (Phase Diagram) for the BaV_2O_6-$Sr_{1-x}Ba_xNb_2O_6$ system. A pseudo-eutectic occurs at 15 mole% of $Sr_{1-x}Ba_xNb_2O_6$, above which the $Sr_{1-x}Ba_xNb_2O_6$ phase was crystallized. The saturation temperature, i.e., the liquidus temperature for the pure $Sr_{1-x}Ba_xNb_2O_6$ phase,

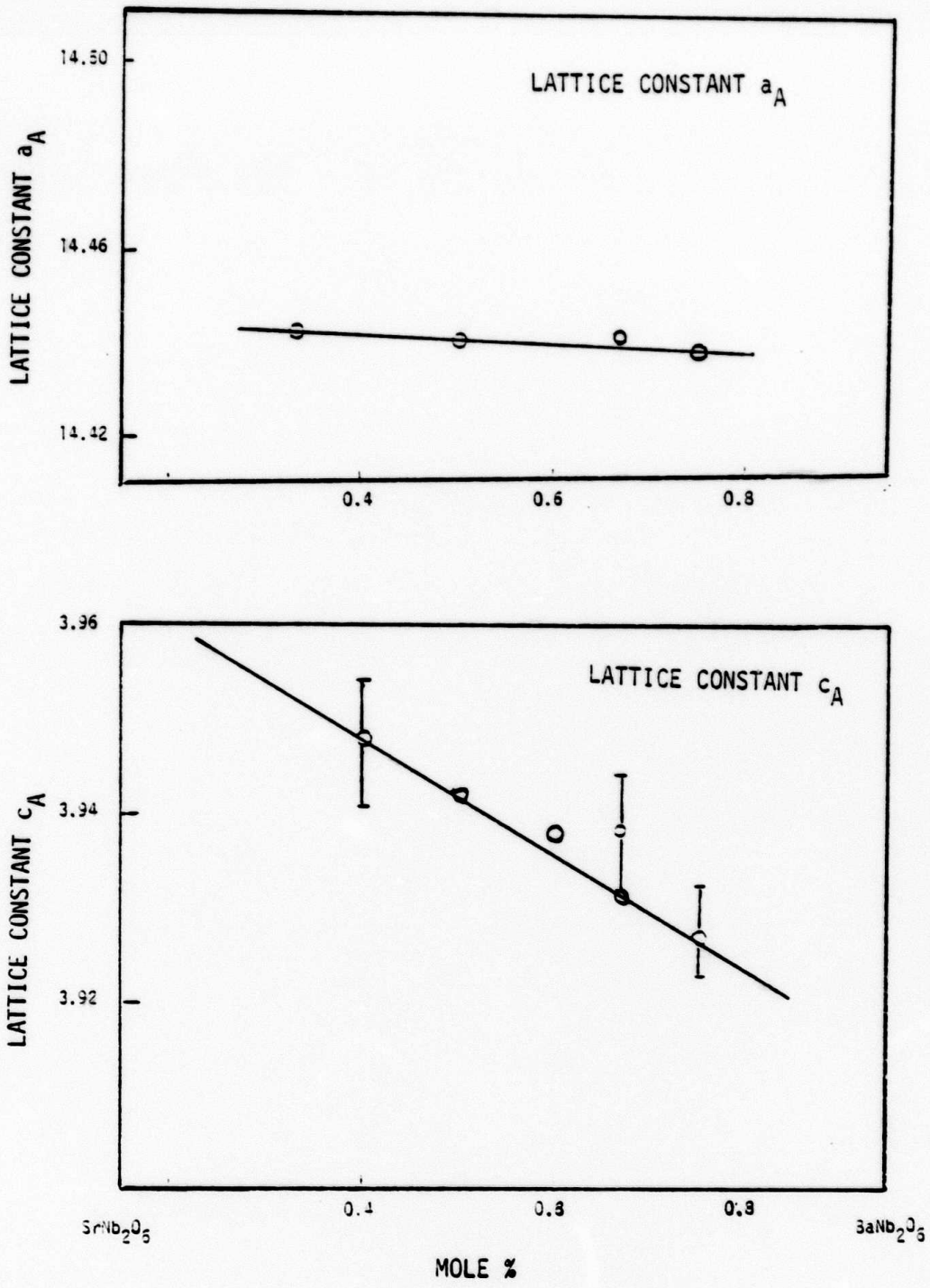

Fig. 3 Lattice constants as a function of composition for the $Sr_{1-x}Ba_xNb_2O_6$ system.

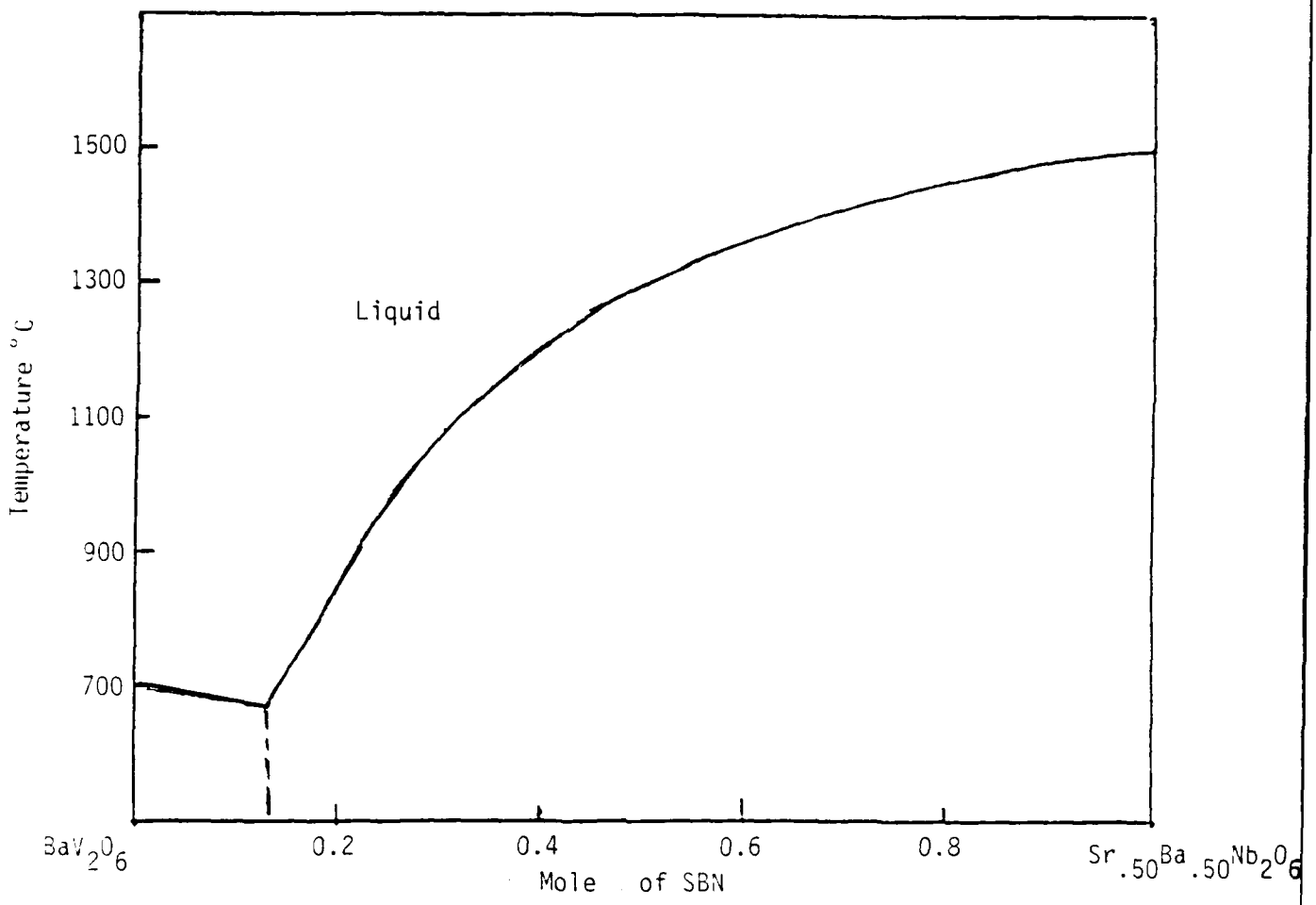

Fig. 4 Phase diagram of the BaV_2O_6-$Sr_{1-x}Ba_xNB_2O_6$ pseudo-binary system.

is between 750 to 1500°C. The supercooling range for the system is about 10 to 15°C, which will be very useful for the thin film growth work.

The system BaB_8O_{13}-$Sr_{1-x}Ba_xNb_2O_6$ has also been found to be very useful for the thin film growth work and further work on this system is in progress (DTA work). The results of this study clearly indicate that both these systems are useful for the thin film growth work and will play important roles in this investigation.

The systems KVO_3-$Sr_{1-x}Ba_xNb_2O_6$ and $NaVO_3$-$Sr_{1-x}Ba_xNb_2O_6$ were examined carefully and it was found that, although the tetragonal tungsten bronze phase was crystallized on both the systems, the composition of the phase was different in each case. $Sr_2KNb_5O_{15}$ and $Sr_2NaNb_5O_{15}$ types of bronze phases were identified. Both these phases belong to the tetragonal bronze structure and are useful ferroic materials.

The remaining two flux systems, $LiVO_3$-$Sr_{1-x}Ba_xNb_2O_6$ and Li_2WO_4-$Sr_{1-x}Ba_xNb_2O_6$ did not produce a stable composition of $Sr_{1-x}Ba_xNb_2O_6$ until 75 mole% of $Sr_{1-x}Ba_xNb_2O_6$, and would require a dipping temperature of at least 1300°C. $LiNbO_3$ was found to be a major phase on these systems, and we conclude these fluxes are not suitable in the present work.

In summary, of the total number of flux systems investigated for the liquid phase epitaxy growth of $Sr_{1-x}Ba_xNb_2O_6$, barium vanadte, strontium vanadate and barium borate systems were found to be the most desirable for this task. The LPE growth experiment has been initiated using the BaV_2O_6-$Sr_{1-x}Ba_xNb_2O_6$ system and the Z-cut SBN substrates. The main emphasis in the coming year will be to develop epilayers of the SBN compositions and new bronze phases having high coupling constants and temperature compensated orientations.

Table III

Phase Analysis of the BaV_2O_6-$Sr_{1-x}Ba_xNb_2O_6$ System

Composition	Phases Present	Remarks
BaV_2O_6-$SrNb_2O_6$	SBN*	$Sr_{.60}Ba_{.40}Nb_2O_6$
BaV_2O_6-$Sr_{.80}Ba_{.20}Nb_2O_6$	SBN	$Sr_{.60}Ba_{.40}Nb_2O_6$
BaV_2O_6-$Sr_{.60}Ba_{.40}Nb_2O_6$	SBN	$Sr_{.50}Ba_{.50}Nb_2O_6$
BaV_2O_6-$Sr_{.50}Ba_{.50}Nb_2O_6$	SBN	$Sr_{.50}Ba_{.50}Nb_2O_6$
BaV_2O_6-$Sr_{.40}Ba_{.60}Nb_2O_6$	SBN	$Sr_{.45}Ba_{.55}Nb_2O_6$
BaV_2O_6-$Sr_{.30}Ba_{.70}Nb_2O_6$	SBN	$Sr_{.35}Ba_{.65}Nb_2O_6$
BaV_2O_6-$Sr_{.25}Ba_{.85}Nb_2O_6$	SBN + $BaNb_2O_6$**	--
BaV_2O_6-$Sr_{.15}Ba_{.85}Nb_2O_6$	$BaNb_2O_6$	--
BaV_2O_6-$BaNb_2O_6$	$BaNb_2O_6$	--

SBN* → tetragonal tungsten bronze phase $Sr_{1-x}Ba_xNb_2O_6$.
$BaNb_2O_6$** → does not belong to the tungsten bronze family.

4.1.3 Bulk Crystal Growth of the $Sr_{1-x}Ba_xNb_2O_6$ Compositions by the Czochralski Technique

This bulk crystal growth program has been supported by the internal (IR&D) funding to provide continuous supply of substrate materials for the LPE work proposed in the present project.

Most recent data from the literature[7] indicate that the composition $Sr_{.61}Ba_{.39}Nb_2O_6$ is only congruently melting composition of the entire series, e.g., $Sr_{1-x}Ba_xNb_2O_6$, $0.25<x<.75$. This suggests that a crystal should be pulled from the composition $Sr_{.61}Ba_{.39}Nb_2O_6$ to obtain striation-free crystals. The melting temperature for this series is ~1500°C, and one can use either iridium or platinum crucible for the growth experiments.

Initially, the crystals were pulled on a platinum wire in Ar atmosphere. It was found that the crystals had a tendency to grow along the c-axis corresponding to the crystal puller. The crystal obtained by using platinum wire were oriented and cut in to seed crystals, which were used for further pulling experiments. To date, it is possible to produce 1/2 inch in diameter and 4 inch long crystals. This is a significant accomplishment in the present work, and we expect to produce still bigger size crystals. The crystals are large enough to initiate the LPE work on these crystals.

C-axis grown boules were cut and the wafers were approximately 1 mm in thickness with c-axis normal to the major surface. The wafers were then electroded using 50Å of chrome and 2000Å of gold. The Curie temperature was measured by monitoring wafer capacitance and conductivity as a function of temperature over the range 25 to 150°C. For a composition of SBN-61 (61% Sr), the Curie temperature was approximately 72°C. The wafers were poled by applying approximately 15 kV/cm at 60°C for 30 minutes.

Exceptionally strong piezoelectric activity was observed in all poled samples. To measure piezoelectric coupling, the wafer was mounted in a 50Ω transmission fixture and RF transmission observed over the range 0 to 10 MHz with an HP3570 network analyzer. Plotted is the strength of mode vs the frequency of series resonance, f_R. Coupling K was calculated from a measurement of series resonance and anti-resonance, f_A frequency.

$$k = \sqrt{\frac{f_A^2 - f_R^2}{f_R^2}}$$

Coupling strengths were typically greater than 10% for both fundamental shear and longitudinal modes. Future work will explain the observed mode spectra of Fig. 5 in terms of elastic and piezoelectric constants, using the well known elastic wave equation and Maxwell's equations. In addition, surface wave devices will be tested on SBN, and the SAW velocity compared to calculations based upon the above elastic constants.

4.2 Crystal Chemistry

4.2.1 Structural Information of the Tungsten Bronze Family

The tungsten bronze (T.B.) structure is characterized by the network of octahedra sharing the corners, and it would be safely said that this structure stands intermediate positions between the perovskite and pyrochlore-type structures. The tetragonal bronze unit cell is shown in Fig. 6 in the projection of the (001) plane and can accommodate metal ions in five different sites designated A_1, A_2, C, B_1 and B_2. Most of the bronze compounds and solid solutions belong to the tetragonal bronze structure. The structure basically consists of a complex array of distorted BO_6 octahedra sharing corners in such a way that there are three different types of interstices between them, which are available for cation occupation. These three types of sites are referred to as follows:

A_1 sites in the pentagonal tunnels parallel to c-axis of which there are four per unit cell, each surrounded by 15-oxygen atoms.
A_2 sites in the tetragonal tunnels parllel to the c-axis of which there are two per unit cell, each surrounded by 12-oxygen atoms.
C sites in the trigonal channels parallel to the c-axis of which there are four per unit cell, each surrounded by 9-oxygen atoms.
B_2 sites surrounded by the A_2 sites, while B_1 sites are located at the center of the unit cells rectangular faces.

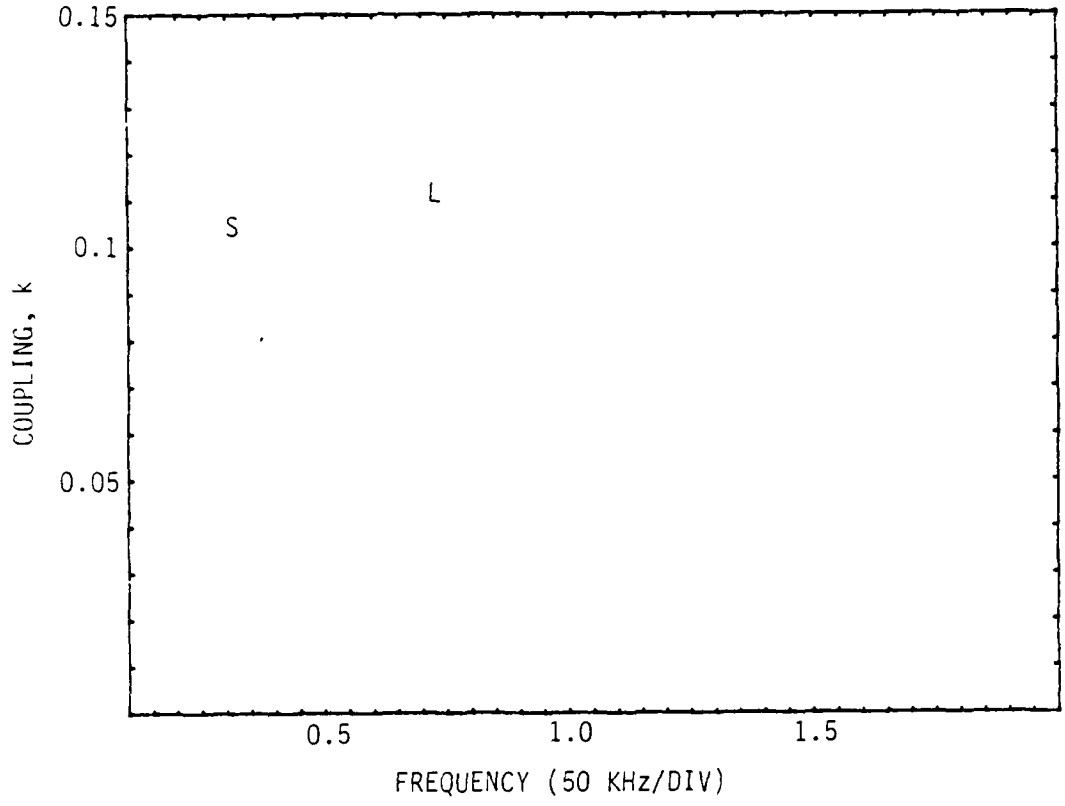

Fig. 5 Strength of mode as a function of the frequency.

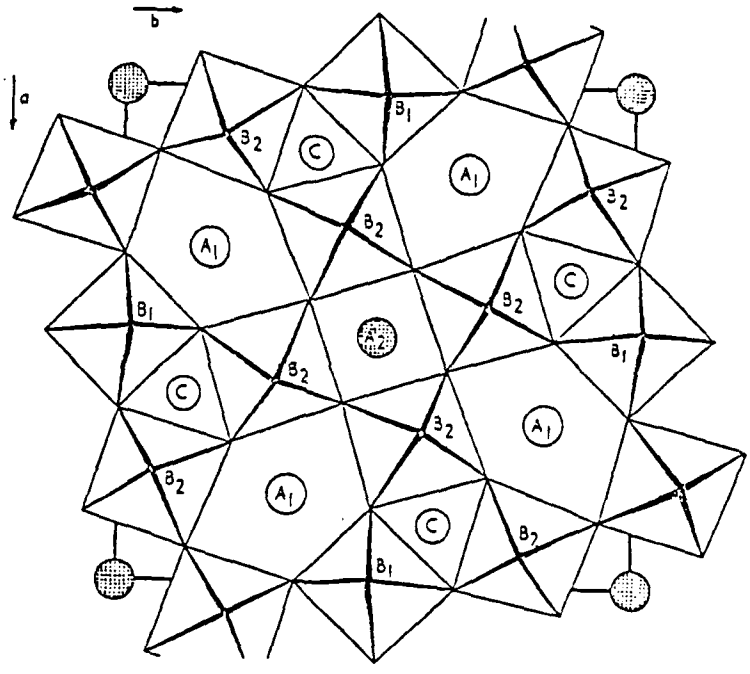

Fig. 6 The tetragonal tungsten bronze unit cell of the structure $(A_1)_4(A_2)_2C_4(B_1)_2(B_2)_8O_{30}$.

The unit cell formula may thus be described as $(A_1)_4(A_2)_2C_4(B_1)_2(B_2)_8O_{30}$. As shown in Table IV, a wide variety of substitutions are possible in the various sites of bronze structure. The tungsten bronze family embraces 80 or more known compounds and solid solution systems (Given in Tables 1 a-d). Within this extensive group, several members have high Curie temperatures, high coupling coefficients and temperature compensated orientations. Ferroelectric: Ferroelastic transitions are known to occur, and a very wide range of mutual solid solubility between end members is possible.

It is clear that although the bronze family is vast and complex, it offers an opportunity to develop bronze compositions of desired structural and physical properties for various applications such as electro-optic, pyroelectric, or as temperature compensated devices. In the present study, we picked the tetragonal $Sr_{1-x}Ba_xNb_2O_6$ and orthorhombic $PbNb_2O_6$ bronze compounds as prototype host, and efforts are being made to improve or alter their properties by adding specific impurities. The tetragonal $Sr_{1-x}Ba_xNb_2O_6$ solid solution itself is very useful for several device appliations. $Sr_{.75}Ba_{.25}Nb_2O_6$ has the largest electro-optic[8] and pyroelectric coefficient[9] of any well-behaved materials. According to unpublished work by Cross,[10] $Sr_{1-x}Ba_xNb_2O_6$ solid solution possesses temperature compensated orientations.

4.2.2 Preparation of New Bronze Solid-Solutions

The substitutions were made in the chosen host materials as follows:

1) $(1-x)\ M^{2+}Nb_2O_6 + x\ M^{3+}_{.5}M^{+}_{.5}Nb_2O_6 \text{ ---- } M^{2+}_{1-x}M^{+}_{x}M^{3+}_{x}Nb_2O_6$

where M^{2+} = Sr, Ba or Pb

M^{+} = K, Na or Li

M^{3+} = Y, Bi or rare earths

Table IV

Ions that Enter Various Sites of the Tungsten Bronze Structure

Crystallographic Site	Cations
SITE - A_1	Rb^+, Ti^+, Cations M-O-M
C.N. = 15	(M = Nb, Ta, Mo or W)
SITES A_1 and A_2	Na^+, K^+, Ag^+
C.N. = 15 and 12	Ca^{2+}, Sr^{2+}, Ba^{2+}, Eu^{2+}, Pb^{2+}
	Y^{3+}, La^{3+}, Ce^{3+}, Pr^{3+}, Nd^{3+}, Sm^{3+}, Eu^{3+}, Gd^{3+}
	Tb^{3+}, Dy^{3+}, Ho^{3+}, Yb^{3+} and Bi^{3+}
SITE - A_2	Cd^{2+}
C.N. = 12	
SITE - C	Li^+, Mg^{2+} and Al^{3+} etc.
C.N. = 9	
SITES B_1 and B_2	Li^+, Mg^{2+}, V^{2+}, Fe^{2+}, Co^{2+}, Ni^{2+}, Cu^{2+}, Zn^{2+}
C.N. = 6	V^{3+}, Mn^{3+}, Fe^{3+}, Ti^{4+}, Zr^{4+}, Sn^{4+}, Nb^{4+}
	V^{5+}, Nb^{5+}, Ta^{5+}, W^{5+}
	Mo^{6+}, W^{6+}
Anion Site	F^-, O^{2-}

2) $(1-x)\ M^{2+}Nb_2O_6 + \frac{x}{2} M_2^{3+}M_2^{4+}O_7 \quad \text{----} \quad M^{2+}_{1-x}M^{3+}_{x}Nb_{2-x}M^{4+}_{x}\ O_6$

where M^{3+} = La, Bi or Gd
M^{4+} = Ti, Zr or Sn.

All of the materials are prepared by the solid state technique using analytical grade materials. After calcining around 800-1000°C for four hours, each batch mixture was ball-milled in acetone for four hours, dried and pressed into disks. The disks were sintered at 1350-1400°C for 10-15 hours in air. Following these procedures, x-ray diffraction techniques were used to identify phase purity and to determine the lattice constants for the different tetragonal tungsten-bronze solid-solutions observed.

The results of the x-ray powder diffraction measurements indicated that the substitution of $M_{.5}^{3+}M_{.5}^{+}Nb_2O_6$ and $M_2^{3+}M_2^{4+}O_7$ phases is possible in all the metaniobates $M^{2+}Nb_2O_6$ and introdued the tetragonal tungsten bronze solid solution in all systems studied. $K_{.5}La_{.5}Nb_2O_6$ is isostructural with the para-electric phase of $PbNb_2O_6$, while $M_2^{3+}M_2^{4+}O_7$ belongs to the pyrochlore structural family. Both theses systems can be represented as $M^{2+}Nb_2O_6$-$M_{.5}M_{.5}Nb_2O_6$ and $M^{2+}Nb_2O_6$-$M_2^{3+}M_2^{4+}O_7$.

The crystalline solid solubility of $BaNb_2O_6$-$K_{.5}La_{.5}Nb_2O_6$ was studied in detail and the results of this investigation has been presented in Fig. 7. although both the $BaNb_2O_6$ and $K_{.5}La_{.5}Nb_2O_6$ phases do not belong to the tungsten bronze family, the addition of $K_{.5}La_{.5}Nb_2O_6$ in $BaNb_2O_6$ introduced the tetragonal tungsten bronze solid solution over a wide compositional range, and it extends between $0.25<x<0.65$. All the phases were well crystallized and can be easily indexed on the tetragonal bronze structure. The replacement of K^+ by Na^+ in $Ba_{.50}K_{.25}La_{.25}Nb_2O_6$ has been accomplished. Similarly, the substitution of other rare-earths such as Eu^{3+}, Gd^{3+}, Dy^{3+} or Ho^{3+} and Y^{3+} or Bi^{3+} was successful in both the $Ba_{.50}K_{.25}La_{.25}Nb_2O_6$ and $Ba_{.50}Na_{.25}La_{.25}Nb_2O_6$ compositions. Although the substitution of Li^+ in the tungsten bronze structure is known,[11,12] e.g., $K_3Li_2Nb_5O_{15}$ and $K_3Li_2Ta_5O_{15}$, the synthesis of $Ba_{.50}Li_{.25}La_{.25}Nb_2O_6$ was successful.

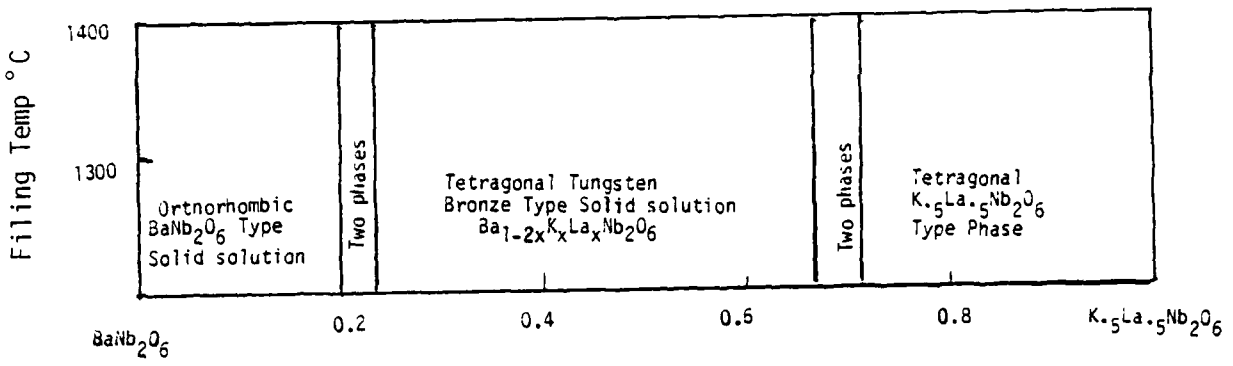

Fig. 7 Phases in the system $Ba_{1-2x}K_xLa_xNb_2O_6$ as observed at room temperature.

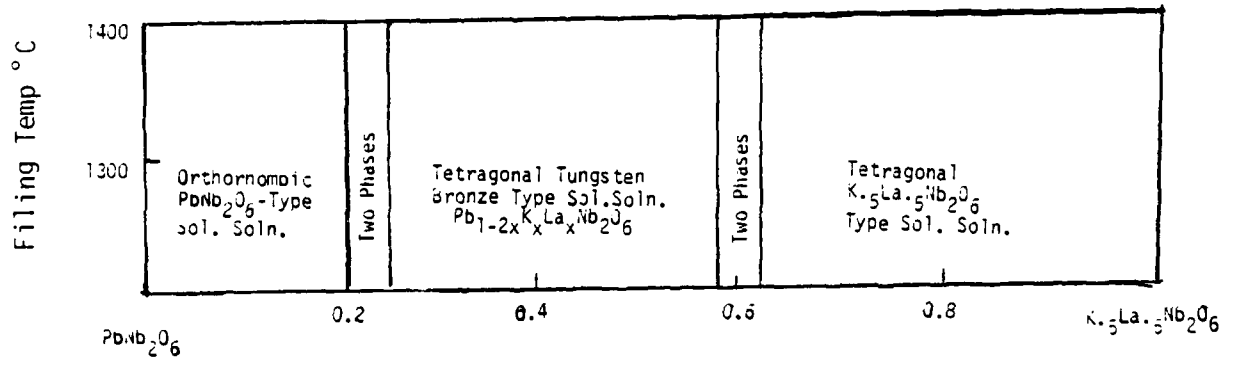

Fig. 8 Phases in the system $Pb_{1-2x}K_xLa_xNB_2O_6$ as observed at room temperature.

$PbNb_2O_6$ belongs to the tungsten bronze family and has an orthorhombic unit cell at room temperature. As shown in Fig. 8, it is interesting to note that both the orthorhombic and tetragonal tungsten bronze phases exist on the $PbNb_2O_6$-$K_{.5}La_{.5}Nb_2O_6$ system. A similar situation has also been reported for the $Pb_{1-x}Ba_xNb_2O_6$ solid solution system.[13] This system appears to be most attractive for the undertaken work, since both the orthorhombic and tetragonal ferroelectric phases co-exist in the same system. The replacement of K^+ by Na^+ and La^{3+} by Gd^{3+}, Eu^{3+} or Bi^{3+} has been shown to be successful in the present system.

For the second type of system, $Ba_{1-x}La_xNb_{2-x}M^{4+}O_6$, where M = Ti, Zr or Sn, tetragonal tungsten bronze solid-solution have been reported. Figure 9 shows the results of the present work on the $BaNb_2O_6$-$La_2Zr_2O_7$ system. The crystalline solid solubility of M^{3+} and M^{4+} ions is, however, limited as compared to the solid solubility of M^+ and M^{3+} ions. The tetragonal tungsten bronze structure exists in the compositional range $0.15<x<0.40$ on the $Ba_{1-x}La_xNb_{2-x}Zr_xO_6$ system. The substitution of Ti^{4+} as $Ba_6Ti_2Nb_8O_{30}$ is known to exist in this family;[14] however, Zr^{4+} and Sn^{4+} containing tungsten bronze phases are not known. The incorporation of Zr^{4+} and Sn^{4+} may play a significant role in this structure.

4.2.3 Dielectric Data

The Curie temperature, T_c, is known to be one of the fundamental characteristics of ferro- and anti-ferroelectrics. This measurement gives the origin of the spontaneously polarized state, and is considered important for characterizing the piezoelectric materials. In the present work, the T_c for the different solid-solution systems has been obtained by measuring the dielectric properties as a function of temperature. The technique is relatively simple and the measurements are made routinely using a capacitance bridge (HP4270A). The test samples (disks) used for the dielectrical measurements are approximately 1.3 cm in diameter and .3 cm inches thick, and coated on each side with platinum by the standard vacuum evaporation technique.

The T_c was measured for the tetragonal bronze solid-solutions having

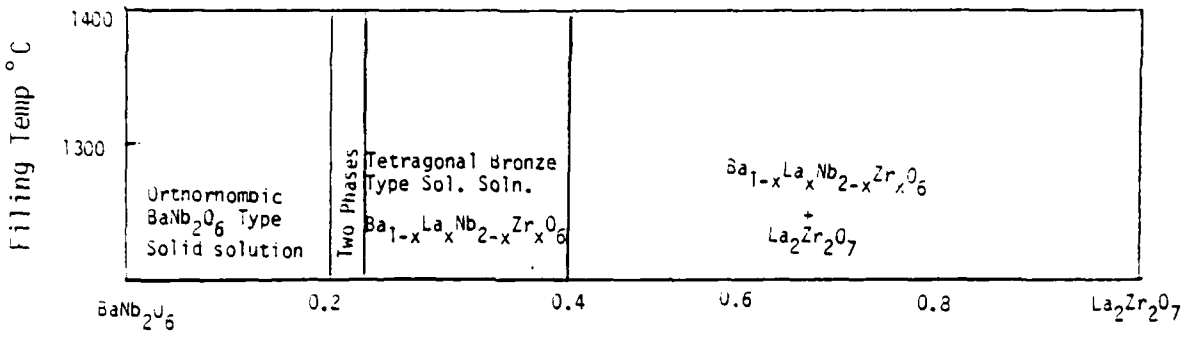

Fig. 9 Phases in the system $Ba_{1-x}La_xNb_{2-x}Zr_xO_6$ as observed at room temperature.

compositions $Ba_{1-2x}K_xLa_xNb_2O_6$ and $Ba_{1-x}La_xNb_{2-x}M^{4+}O_6$, where M = Ti or Zr. the T_c occurred below room temperature and it varied with composition between -110°C to -20°C for both systems. The results are reproducible and these findings are consistent with the results reported for the Ti^{4+} containing bronze phases,[14] e.g., $Sr_5BiTi_3Nb_7O_{30}$ (T_c = -10°C), $Ba_3La_3Ti_5Nb_5O_{30}$ (T_c = -130°C), and $Ba_4Bi_2Ti_4Nb_6O_{30}$ (T_c = -31°C). However, it is interesting to note that La^{3+} and Bi^{3+} free tetragonal bronze phases having compositions $Ba_6Ti_2Nb_8O_{30}$ (T_c = 245°C) and $Ba_5KNb_9TiO_{30}$ (T_c = 290°C) had their T_c above 200°C.[14] The work on the other systems is in progress and we expect that some of these phases will be useful for the undertaken work.

$PbNb_2O_6$ is an interesting ferroelectric material, and exhibits the ferroelectric phase transition around 570°C.[14-17] The dielectric measurements on the orthorhombic solid-solution, $Pb_{1-2x}K_xLa_xNb_2O_6$ have already been made, and it was found that the addition of $K_{.5}La_{.5}Nb_2O_6$ in $PbNb_2O_6$ favors the T_c shift towards a lower temperature. The T_c shift is moderate for this system and the T_c remains above room temperature for the samples studied. The measurements on the tetragonal bronze solid-solution, $Pb_{1-2x}K_xLa_xNb_2O_6$, are also in progress.

5.0 FUTURE PLANS

5.1 LPE Growth and Characterization of Bronze Phases

During the second year of this contract, the LPE process will be established for the SBN compositions using the flux systems described in Section 4.1.2. Once this technique is developed, the process will be applied to other tungsten bronze compositions having high coupling constants and temperature compensated orientations. Studies will be made in characterizing the bulk single crystals, as well as thin films of bronze compositions in terms of its piezoelectricity and temperature dependence of surface acoustic wave for given direction of propagation.

5.2 Crystal Chemistry

The work on the $M^{2+}Nb_2O_6$-$K_{.5}M^{3+}Nb_2O_6$ and $M^{2+}Nb_2O_6$-$M_2^{3+}M_2^{4+}O_7$, where M^{2+} = Pb, Sr or Ba; M^{3+} = La, Gd, Y, Dy or Bi and M^{4+} = Zr, Ti or Sn, will be continued to prepare new tetragonal and orthorhombic tungsten bronze solid-solutions. The selected compositions from these systems will be studied in detail to obtain the dielectric, piezoelectric and thermal expansion data before they are tried for the LPE work.

5.3 Application of Phenomenological Model

The phenomenological model derived at the Pennsylvania State University will be applied to determine the composition of SBN epitaxial films to give large electromechanical coupling and still reamin temperature compensated. In order to ascertain the validity of the phenomenological model, sixth order electrostrictive constants for SBN hve to be experimentally determined. These constants are important in relating to the polarization dependent on acoustic wave velocity, the magnitude of electromechanical coupling constant, and temperature dependent of the acoustic wave velocities.

6.0 PUBLICATIONS

1. R.R. Neurgaonkar, T.C. Lim, E.J. Staples and L.E. Cross, "An Exploration of the Limits of Stability of th $LiNbO_3$ Structure Field with A and B Site Cation Substitutions," Ferroelectric Journal (to appear).

2. K.L. Keester, R.R. Neurgaonkar, T.C. Lim and E.J. Staples, "Strontium Metaniobates: Its Crystallography, Polymorphism and Isomorphism," Materials Res. Bull. (to be published).

3. K.L. Keester and R.R. Neurgaonkar, "Consopic Optics for Characterization of High Refractive Index Uniaxial Materials," submitted to J. of Electronic Materials.

4. R.R. Neurgaonkar, T.C. Lim,E.J. Staples and L.E. Cross, "Structural and Dielectric Properties of $Pb_{1-2x}M^{3+}{}_xNb_2O_6$ and $Pb_{1-x}M^{3+}Nb_{2-x}M^{4+}O_6$ Systems," (in preparation).

PRESENTATIONS

1. K.L. Keester, R.R. Neurgaonkar, T.C. Lim and E.J. Staples, "Conoscopic Characterization of Czochralski-Growth Strontium Barium Niobates Boules," presented at the 4th Conf. on Crystal Growth, Stanford Sierra Camp, Fallen Leaf Lake, California, May 16-18, 1979.

2. R.R. Neurgaonkar, T.C. Lim, E.J. Staples and L.E. Cross, "An Exploration of the Limits of Stability of the $LiNbO_3$ Structural Field with A and B Site Cation Substitutions," presented at the IEEE Int. Symp. of Ferroelectrics, Minneapolis, Minn., June 13-15, 1979.

7.0 REFERENCES

1. L.A. Shuvalov, "Symmetry Aspects of Ferroelectricity," J. Phys. Soc. Japan (Supplement) 28, 38 (1970).

2. R. Roy and W.B. White, "High Temperature Solution and High Pressure Crystal Growth," J. Cryst. Growth 33, 314 (1968).

3. E.J. Staples, R.R. Neurgaonkar and T.C. Lim, "Temperature Coefficient of SAW Velocity on Epitaxial $Li_{1-x}Na_xNbO_3$ Thin Films," Appl. Phys. Lett. 32(4), 197 (1978).

4. A.A. Ballman, H. Brown, P.K. Tien and S. Rive-Sanseverino, "The Growth of $LiNbO_3$ Thin Films by LPE Techniques," J. Cryst. Growth 29, 289 (1975).

5. A. Baudrant, H. Vial and J. Davel, "LPE of $LiNbO_3$ Thin Films for Integrated Optics," Mat. Res. Bull. 10, 1373 (1975).

6. A.A. Ballman and H. Brown, "The Growth and Properties of Strontium Barium Metaniobate, $Sr_{1-x}Ba_xNb_2O_6$: A Tungsten Bronze Ferroelectric," J. Cryst. Growth 1, 311 (1967).

7. K. Megumi, N. Nagatsuma, Y. Kashiwada and Y. Furuhata, "The Congruent Melting Composition of Strontium Barium Niobate," J. Mat. Sci. 11, 1583 (1976).

8. P.L. Lanzo, E.G. Spence and A.A. Ballman, "Electro-Optic Coefficient of Ferroelectric Strontium Barium Niobate," Appl. Phys. Lett. 11, 23 (1967).

9. A.M. Glass, "Investigation of Electrical Properties of $Sr_{1-x}Ba_xNb_2O_6$ With Special Reference to Pyroelectric Detector," J. Appl. Phys. 40, 4699 (1969).

10. L.E. Cross, Private and unpublished communication.

11. T. Fukuda, "Growth and Crystallograhic Characteristics of $K_3Li_2Nb_5O_{15}$ Single Crystals," Jap. J. Appl. Phys. 8, 122 (1969).

12. J. Ravez, A. Perron-Simon and P. Hagenmuller, "Les Phases de Structure Bronzes de Tungstene Quadratiques," Ann. Chim. t1 251, 1976.

13. M.H. Francombe, "The Relation Between Structure and Ferroelectricity in Lead-Barium and Barium-Strontium Niobate," Acta. Cryst. 13, 131 (1960).

14. N.C. Stepheson, "The Crystal Structure of the Tetragonal Bronze $Ba_6Ti_2Nb_8O_{30}$," Acta. Cryst. 18, 496 (1965).

15. Par PH Labbe, M. Frey and G. Allais, "Nouvells Donnees Structurales sur la Variete Ferroelectrique du Metaniobate de Plomb $PbNb_2O_6$," Acta. Cryst. B29, 2204 (1973).

16. E.C. Subbarao, G. Shirane and F. Jone, "X-Ray, Dielectric and Optical Study of Ferroelectric Lead Metaniobate and Related Compounds," Acta. Cryst. 13, 226 (1960).

17. H. Brusset, Mme. H. Gillier-Pandraud, R. Mahe and S.D. Voliotis, "Etude de Systemes Binaries et Pseudo-Binaries Definis Entre Nb_2O_5 et PbO, BaO, SrO," Mat. Res. Bull. 6, 413 (1971).